# Pattern Formation in the Belousov−Zhabotinsky Reaction with Photochemical Global Feedback

**Vladimir K. Vanag,* Anatol M. Zhabotinsky, and Irving R. Epstein**

*Department of Chemistry and Volen Center for Complex Systems, MS 015, Brandeis University, P.O. Box 549110, Waltham, Massachusetts 02454-9110*

*Received: July 5, 2000; In Final Form: October 12, 2000*

We have found a variety of oscillating patterns in the Belousov−Zhabotinsky (BZ) reaction−diffusion system with global negative feedback. Bulk oscillations and wave patterns arise at low values of the feedback strength. When the feedback exceeds a critical value, cluster patterns arise. Besides the standing, irregular, and localized clusters observed earlier, we have found new types of clusters: three-phase, localized irregular, and localized oscillatory clusters. A model of three identical Oregonators with global negative coupling yields the same bifurcation scenario as found in our experiments.

## I. Introduction

Spatially extended nonequilibrium systems with global negative feedback (GNF) have recently drawn significant attention. They are found in heterogeneous catalysis, where exchange through the gas phase globally couples sites on the catalytic surface. They serve as models of neural networks. Many types of spatial patterns have been found in theoretical and experimental studies of chemical systems with GNF.[1−19] Antiphase oscillations were first discovered in the electrochemical dissolution of nickel under galvanostatic conditions.[11] Later, antiphase oscillations of fixed spatial domains were seen in other electrochemical systems with global feedback.[2,7,9,19,20] Oscillatory standing patterns have been found in catalytic systems with global coupling, such as oxidation of CO on Pt,[4,10,17,21] oxidation of hydrogen on Ni,[8,18] methylamine decomposition on Rh,[3] and oxidation of propylene on Pt.[16]

However, experimental data on standing waves and oscillatory clusters in two-dimensional extended chemical systems are quite limited. Homogeneous oscillatory systems are very convenient for study of nonequilibrium chemical pattern formation. Oscillatory standing patterns (OSP) have been found in the $Ru(bpy)_3$-catalyzed BZ reaction subjected to periodic illumination.[22] The same photosensitive BZ reaction was used in the first experiments on OSP in autonomous, homogeneous, reaction−diffusion systems with global negative feedback.[23] In this system, an increase in the average concentration of $Ru(bpy)_3^{3+}$ results in increasing the intensity of the actinic light, which produces bromide ions and inhibits the oxidation of $Ru(bpy)_3^{2+}$. Three types of OSP were found: standing, irregular, and localized clusters. These patterns consist of multiple spatial domains that display antiphase oscillations. Standing clusters (SC) are characterized by periodic antiphase oscillations in neighboring fixed spatial domains. Irregular clusters (IC) consist of oscillatory antiphase domains, which change their shape and position randomly. Localized clusters (LC) contain fixed oscillatory antiphase domains that cover only part of the medium, while the remaining area displays no visible patterns. We refer to these three types as the base cluster patterns. Transitions between base clusters can be induced by changing the strength of the photochemical global feedback.

In this paper, we present a detailed study of pattern formation in the quasi-two-dimensional BZ reaction−diffusion system with photochemical feedback. We show that besides the base clusters there are other types of oscillatory cluster patterns. The appearance of these clusters and the transitions between them depend on the initial reagent concentrations, the target point of the system, and the strength of the feedback. We also show that the experimentally found scenario of cluster−cluster bifurcations may be reproduced in a mathematical model consisting of three identical Oregonators globally coupled by negative feedback.

## II. Experimental Section

Figure 1a shows a block diagram of the experimental setup. In Figure 1b we see a schematic of the one-sided continuously fed unstirred reactor (CFUR), which consists of a continuously stirred tank reactor (CSTR) described earlier [24] and a thin layer of silica gel [25−27] polymerized directly on the front window of the CSTR. The gel contains the immobilized catalyst $Ru(bpy)_3^{2+}$. The one-sided CFUR allows us to reduce significantly the concentration gradients of the initial reactants in the gel layer. The front window and the disk of immobilized silica gel are 22 mm in diameter. A ring diaphragm (D) of inner diameter 14 mm, which is placed in front of the reactor window, determines the working area illuminated by the analyzing light.

The silica gel with $Ru(bpy)_3^{2+}$ is prepared as follows: 90 $\mu$L of $H_2O$, 110 $\mu$L of 0.01 M tris(2,2′-bipyridyl)ruthenium(II) chloride hexahydrate (Aldrich), 94 $\mu$L of 2 M $H_2SO_4$, and 206 $\mu$L of 1.067 M (11.3%) $Na_2SiO_3$ (10 g $Na_2SiO_3 \times 9\ H_2O$ + 28 mL $H_2O$) are mixed and thoroughly stirred in a small cell, then a portion of the mixture is dropped on the horizontally positioned optical window of the CSTR. To vary the gel thickness $h$, we change the volume of the mixture dropped on the window from 82 $\mu$L (0.2 mm thick gel) to 328 $\mu$L (0.8 mm). In most of our experiments we use silica gel with $h = 0.412$ mm and $[Ru(II)]_0 = 2.2$ mM. The photoresponse of the BZ system in a gel depends on the gel thickness and has a bell-shaped form with a maximum at 0.3−0.4 mm (see Appendix 1). In some experiments we change the concentration of $Ru(bpy)_3^{2+}$ in the gel, while the concentrations of $H_2SO_4$ and $Na_2SiO_3$ in the mixture are kept constant. After 10−12 h of polymerization,

10.1021/jp002390h CCC: $19.00 
Published on Web 11/17/2000

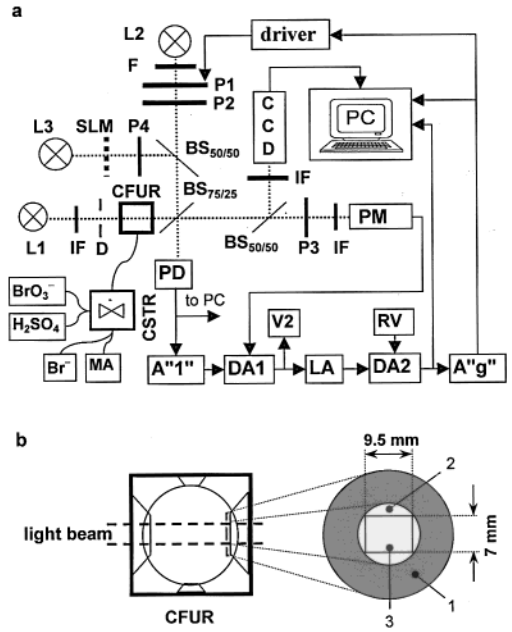


**Figure 1.** (a) Experimental setup. IF is interference filter, D is diaphragm, CFUR is continuously fed unstirred reactor, CSTR is a continuously stirred tank reactor, $BS_{75/25}$ is beam splitter that reflects 75% and transmits 25% of light. P1−P4 are polarizers, PM is photomultiplier, PD is photodiode of powermeter, CCD is digital CCD camera, PC is personal computer, SLM is spatial light modulator (mask). (b) Continuously fed unstirred reactor (CFUR) consists of 20 mL continuously stirred tank reactor (CSTR) thermostated at 25 °C and thin layer of silica gel polymerized on reactor optical window (gray circle 1). Diaphragm (D) selects working area of gel (light gray circle 2). Rectangular frame 3 shows field of view of CCD camera. For other details, see text.

the gel is washed several times in 0.4 M $H_2SO_4$ over the next 10−12 h. The concentration of Ru(II) in the gel decreases by 30−40% during the washing procedure, and is the final concentration $[Ru(II)]_f$ is about1.5 mM. The remaining $Ru(bpy)_3^{2+}$ is fixed in the gel more or less firmly, since the rate of decrease of $[Ru(II)]_f$ is less than 0.1% per hour. The optical density of the gel at $\lambda = 450$ nm is about 0.9 after washing. During the experiment the total concentration of catalyst, [Ru(II)] + [Ru(III)], decreases slowly, which is manifested in a decreasing amplitude of the gel bulk oscillations that start if the light is switched off. The rate of catalyst escape from the gel or catalyst inactivation due to formation of inactive and insoluble complexes of Ru(II) or Ru(III) with $Br_2$ [28] does not exceed 1−2% per hour during the experiment.

A peristaltic pump delivers stock solutions of NaBr, malonic acid (MA), $NaBrO_3$ and $H_2SO_4$ into a premixing chamber and then into the CFUR. In all experiments the initial reagent concentrations correspond to the oscillatory region of the parameter space. The steady-state concentrations of the reagents in the CFUR are calculated according to Försterling et al. [29,30] The results of our calculations of the initial reagent concentrations in the working CSTR are presented in Table 1. The concentrations are arranged in Table 1 in increasing order of the ratio $r$, where $r = k_R[H^+]_f[BrO_3^-]_f/(33(k_M[MA]_f + k_B[BrMA]_f + k_{BB}[Br_2MA]_f))$. This ratio characterizes the distance of the working point from the boundary between the oscillatory and reduced steady-state regions in the space of reagent concentrations. The constants $k_M$, $k_B$, and $k_{BB}$ are the rate constants for the reactions of Ru(III) with malonic acid, bromomalonic acid and dibromomalonic acid, respectively; $k_R$ is the rate constant of production of $BrO_2$ radicals. We use the values $k_R = 33\ M^{-2}s^{-1}$, $k_M = 0.2\ M^{-1}\ s^{-1}$, $k_B = 55\ M^{-1}\ s^{-1}$,[31] $k_{BB} = 0.2\ M^{-1}\ s^{-1}$.[28] The residence time of the CSTR, $k_0^{-1}$ (where $k_0 = v_f/V_0$, $v_f$ is the total flow rate through the CSTR, and $V_0$ is the volume of the CSTR, $V_0 = 20$ mL), strongly affects the steady-state concentration of bromide ions in the CFUR. For example, when $k_0 = 10^{-7}\ s^{-1}$ (close to a batch reactor), $[Br^-]_{SS} = 6 \times 10^{-9}$ M, while for $k_0 = 10^{-3}\ s^{-1}$, $[Br^-]_{SS} = 1.2 \times 10^{-4}$ M for initial concentrations corresponding to cases a−c in Table 1. In most of our experiments, we use $k_0 = 10^{-4}\ s^{-1}$. In some experiments, we change $k_0$ to vary the photosensitivity of the BZ reaction, which increases with the rate of $[Br^-]$ input.[32,33]

Analyzing light from a 45 W tungsten lamp (L1) passes through a set of lenses, an interference filter IF450 with wavelength maximum at $\lambda_{max} = 450$ nm, the diaphragm, the silica gel with the immobilized catalyst in it, two beam splitters ($BS_{75/25}$ and $BS_{50/50}$), polarizer P3, and another interference filter IF450, and is then collected by a photomultiplier (PM). After passing through the silica gel, all the light (except the light reflected by the beam splitters) is collected by a lens and directed to the PM. We thus measure the gel absorption $A_{av}$ averaged over the working area of the silica gel.

The crucial part of the setup is the negative global optical feedback loop. In our system, the intensity of the actinic light increases when the average $[Ru(bpy)_3^{3+}]$ rises, and decreases when it falls. A signal from PM goes through a set of amplifiers and then to a driver that rotates one of the two crossed polarizers, P1. For the intensity of actinic light $I$ incident on the silica gel, the following expressions hold:

$$I = I_{max}\sin^2(\pi/2 - \theta) = I_{max}\sin^2(Kc(U - U_{Ref})) = I_{max}\sin^2(g(Z_{av} - Z_t)) \quad (1)$$

Here $\theta$ is the angle between the principal axes of the polarizers; $I_{max}$ is the maximum intensity of the light from the 450 W arc lamp (L2) passing through a water (heat) filter, band-pass filter (400−500 nm), and beam splitter $BS_{50/50}$ and reflected from beam splitter $BS_{75/25}$; $g$ is the feedback coefficient, which can be changed by varying the gain $K$ of a dc amplifier "g" (A"g"); $c$ is a scaling factor which transforms voltage to angle; $U$ is a signal (measured in V) from the logarithmic amplifier (LA), which is directly proportional to $[Ru(bpy)_3^{3+}]_{av}$; $\Delta U/7$ (V) = $\Delta A_{av} = \Delta[Ru(II)]_{av}h\Delta\epsilon_{450}$; $h$ is the gel thickness; and $\Delta\epsilon_{450}$ is the difference between the extinction coefficients of Ru(II) and Ru(III) at $\lambda = 450$ nm. The angle $\theta$ can vary only between 0 and $\pi/2$ due to mechanical constraints, but the difference ($U - U_{Ref}$) is allowed to be negative. The target point $Z_t$ is set by the reference voltage $U_{Ref}$ (RV). The whole silica gel area, including the working area, is illuminated uniformly (to within better than 2%) through a specially arranged set of lenses.

The intensity of the 45 W tungsten lamp light incident on the silica gel $I_a$ is much smaller than $I_{max}$. Typically, $I_a \cong 0.01I_{max}$, and $I_{max} \cong 4.3\ mW/cm^2$. The intensity of the actinic light is measured by a power meter with a photodiode (PD). $I_a$ is not high enough to suppress bulk oscillations in the silica gel, but is sufficient to observe the image of the gel with the video camera. The image data recording system consists of a monochrome CCD video camera (Javelin Electronics, JE7362) and a personal computer (PC) with a special video card All-in-Wonder Pro. The interference filter IF450 is placed in front of the 135 mm lens of the video camera. A 55 mm extension tube is inserted between the 135 mm lens and the video camera. The image size used is 320 × 240 pixels, eight bits per pixel.

Another source of actinic light (150 W Xe arc lamp, L3) can be used to create a predetermined pattern of initial conditions.

**TABLE 1: Initial Reagent Concentrations (Subscript 0, in M) in Stock Solutions and Final Concentrations (Subscript f, in M) in a CSTR with Silica Gel**

| | $[H_2SO_4]_0$ | $[BrO_3^-]_0$ | $[MA]_0$ | $[Br^-]_0$ | $[H^+]_f$ | $[BrO_3^-]_f$ | $[MA]_f$ | $[BrMA]_f$ | $[Br_2MA]_f$ | $10r$ |
|---|---|---|---|---|---|---|---|---|---|---|
| a | 0.45 | 0.25 | 0.3 | 0.1 | 0.3 | 0.2 | 0.194 | 0.0624 | 0.0438 | 0.173 |
| b | 0.5 | 0.25 | 0.3 | 0.1 | 0.35 | 0.2 | 0.194 | 0.0612 | 0.0444 | 0.205 |
| c | 0.5 | 0.25 | 0.25 | 0.1 | 0.35 | 0.2 | 0.149 | 0.0526 | 0.0487 | 0.239 |
| d | 0.708 | 0.25 | 0.292 | 0.15 | 0.483 | 0.175 | 0.15 | 0.059 | 0.083 | 0.257 |
| e | 0.83 | 0.3 | 0.5 | 0.125 | 0.643 | 0.238 | 0.362 | 0.0887 | 0.0494 | 0.308 |
| f | 0.75 | 0.312 | 0.375 | 0.125 | 0.563 | 0.25 | 0.245 | 0.0731 | 0.0572 | 0.344 |
| h | 0.7 | 0.28 | 0.2 | 0.125 | 0.513 | 0.218 | 0.087 | 0.0382 | 0.075 | 0.524 |
| j | 0.7 | 0.4 | 0.2 | 0.125 | 0.513 | 0.338 | 0.087 | 0.0379 | 0.075 | 0.818 |
| k | 0.83 | 0.208 | 0.116 | 0.125 | 0.643 | 0.146 | 0.017 | 0.0104 | 0.0885 | 1.58 |

The image of a specific mask is focused in the plane of the silica gel. The light from the 150 W arc lamp passes through a water filter, a band-pass filter (400−500 nm), and a polarizer P4.

To protect the photomultiplier tube from the scattered actinic light, we employ crossed polarizers P2−P3, and P4−P3. The remnants of the parasitic light are compensated electronically by using dc amplifier "1" (A"1") and differential amplifier "1" (DA1). The gain of dc amplifier "1" is chosen in such a way that under the condition that $I_a = 0$ (no analyzing light) the signal V2 from differential amplifier "1" is equal to 0 at any intensity of actinic light.

### III. Experimental Results

We employ constant illumination to suppress oxidation of the catalyst and set the uniform initial conditions. When the actinic light is switched off, the system starts to oscillate. Fast phase waves (PW) can be seen during the bulk oscillations. The velocity of the PW depends on the initial reagent concentrations. For cases a−c in Table 1 the velocity of PW is relatively slow. In these cases PW emerge approximately at the center of the gel area and spread to its border. For cases e and f in Table 1, the velocity of PW is quite high, and it is difficult to identify a single site where PW emerge. Sometimes PW arise simultaneously throughout the gel in the form of rapidly spreading and merging spots. For cases h and j in Table 1, the velocity of PW is also high, about 0.1−1 cm/s. The period of damped bulk oscillations in the gel is roughly equal to the period of oscillations in a CSTR under the same conditions. After several tens of oscillations, trigger waves (TW) start at the boundary of the gel. The TW and PW move in opposite directions, with the TW eventually annihilating the PW to leave spiral waves.

Although the $Ru(bpy)_3$-catalyzed BZ reaction under constant illumination has been previously studied both in a CSTR [34−37] and in spatially extended systems,[26,38−41] we briefly present some results under the conditions which are important for understanding how clusters emerge. There are two critical light intensities, $I_1$ and $I_2$, in the oscillatory reaction−diffusion BZ reaction. The first, $I_1$, is the level that suppresses bulk oscillation. The value of $I_1$ depends on the rate of decrease in bromide concentration near $[Br^-]_{cr}$, the critical concentration below which autocatalysis can occur. The other critical intensity, $I_2$, is the minimum intensity of constant illumination sufficient to suppress all waves in the gel. When $I_1 < I < I_2$, wave patterns (e.g., spiral waves) exist in the gel. At $I > I_2$, the system resides in the reduced steady state. The value of $I_2$ depends on the rate of autocatalysis and the diffusion coefficients of the activator ($HBrO_2$) and the inhibitor ($Br^-$), as well as on the gel thickness $h$ and the gel absorption $h\epsilon[Ru(II)]$. The last two values determine the uniformity of $[Br^-]$ along the optical axis and the extent to which a two-dimensional approximation of the real three-dimensional gel is appropriate. Typically, $I_2$ is several times greater than $I_1$. Clusters emerge if the minimum light intensity of the variable actinic light is smaller than $I_1$ (during the oscillation phase when $[Ru(bpy)_3^{3+}]_{av}$ is small) and the maximum of $I$ exceeds $I_2$ (during the oscillation phase when $[Ru(bpy)_3^{3+}]_{av}$ is large).

At small $g$, when $I_{max} \sin^2(\pi/2 - \theta)_{max} < I_2$, various traveling wave patterns (most often scroll waves), which look like splitting or alternating waves in the form of spirals, rings and other geometrical figures, are found in the system. When $I_{max} > I_2$ and $g$ is high enough, all traveling waves are suppressed and standing oscillatory clusters may appear. Note that $I$ defined by eq 1 depends on the initial conditions, since $Z_{av} = [Ru(bpy)_3^{3+}]_{av}$ depends on the initial pattern. If the initial conditions are uniform (e.g., the system is in the reduced steady state) the amplitude of oscillations, $\Delta[Ru(bpy)_3^{3+}]_{av}$, is maximal, since all portions of the medium oscillate in phase. For this case the coefficient $g$ need not be very high in order for $I$ to reach $I_2$ ($I_{max}$, of course, must exceed $I_2$). If the initial conditions are not uniform, $\Delta[Ru(bpy)_3^{3+}]_{av}$ tends to be small and depends on the initial pattern. To obtain standing clusters in this case, $g$ must be higher than in the case of uniform initial conditions. This dependence on initial conditions leads to coexistence of wave patterns and clusters at the same $g$, i.e., bistability.

We present first a family of cluster patterns obtained at several initial reagent concentrations within the oscillatory region of the BZ reaction (see Table 1). These patterns are generated from spatially uniform initial conditions first by an instantaneous increase in the feedback coefficient $g$, and then by varying $g$ after clusters have formed. For cases a−d in Table 1 (parameters close to the Hopf bifurcation line that separates the oscillatory and reduced steady state regions), we obtain standing clusters (SC) and localized clusters (LC). The behavior of a SC during one full period is presented in Figure 2. The brightness of the white domains increases gradually and is proportional to $[Ru(bpy)_3^{3+}]_{av}$. When the light intensity reaches its maximum, the white domains start to fade, and finally the gel returns to its uniform black state. In the next half period, the formerly black regions of the gel become white. In SC, the period, $T_0$, of such global variables as the gel absorption, Abs-450 (Abs-450 = constant$[Ru(bpy)_3^{2+}]_{av}$), or the light intensity $I$ (see bottom panel in Figure 2) is half the period of the local concentration oscillations at each point.

A typical transition from SC to LC is presented in Figure 3a. As $g$ increases, the transition proceeds gradually, with the area of SC, $S_{osc}$, shrinking and the nonoscillatory area (to be more precise, the area with no visible patterns at the right of the rightmost snapshots in Figure 3a), $S_{no}$, spreading. This process is analogous to a second-order phase transition. In Figure 3b, we see that as $g$ grows further, the nonoscillatory (dark) region of LC (at the left of each snapshot) continues to expand. Finally LC give way to small amplitude bulk oscillations at still higher $g$. We did not observe any situation in which $S_{osc} \rightarrow 0$.

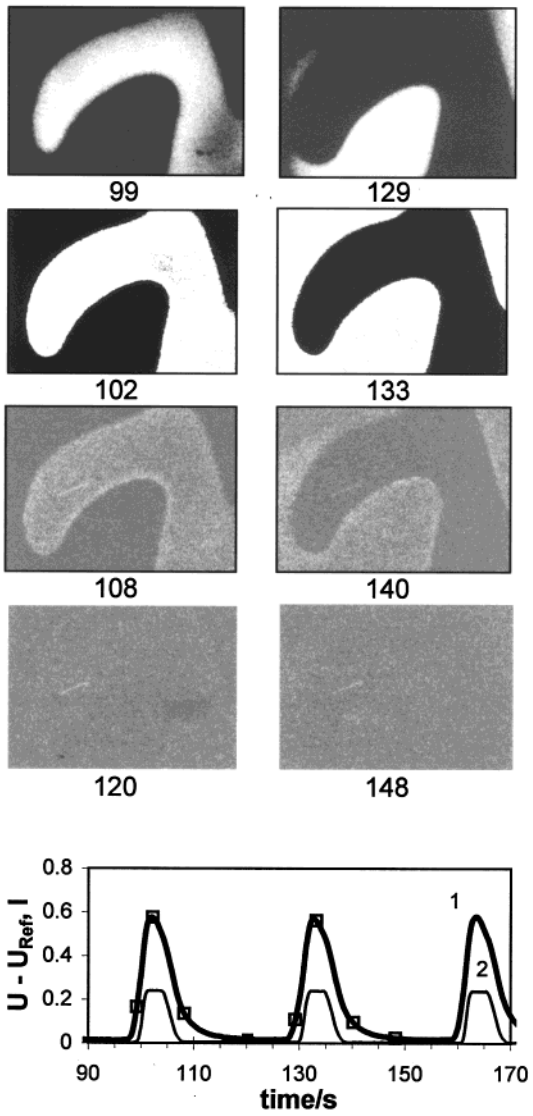


**Figure 2.** One period of oscillation of a standing cluster. Uniform initial conditions were obtained by illuminating gel area for 30 s with constant light from 150 W arc lamp; then feedback (450 W arc lamp) was switched on and simultaneously 150 W lamp was switched off. Gray levels quantify $[Ru(bpy)_3^{3+}]$, with white corresponding to maximum and black to minimum. Numbers under frames show time in s. Initial reagent concentrations correspond to case d in Table 1, $g = 16.2$ mM$^{-1}$. Squares on curve 1 ($(U - U_{Ref})$ in V) indicate times when snapshots were taken; curve 2 is light intensity in relative units.

Instead, there appears to be a finite minimum of $S_{osc}$, $S_{min}$, at which the transition from LC to bulk oscillations occurs.

For cases e and f in Table 1 we obtained 4 types of clusters (initial reagent concentrations lie far from the boundary of the oscillatory region). They are SC, three-phase clusters (3pC), irregular clusters (IC), and localized irregular clusters (LIC) (see Figure 4). Three-phase clusters are characterized by three different spatial areas (black, gray, and white in Figure 4b) corresponding to three different phases of the oscillatory cycle. The transitions from SC to 3pC and from 3pC to IC occur discontinuously as $g$ is increased, as in a first order phase transition. The transition from IC to LIC is analogous to the transition from SC to LC and proceeds gradually. LIC differ from IC by the existence of a fixed area in which white spots never emerge (the upper half of the frame in Figure 4d). In IC, every point of the medium will eventually be covered by a white spot.

Three-phase clusters occur in a narrow range of $g$ between SC and IC. Snapshots taken at intervals of $T_0$, the period of

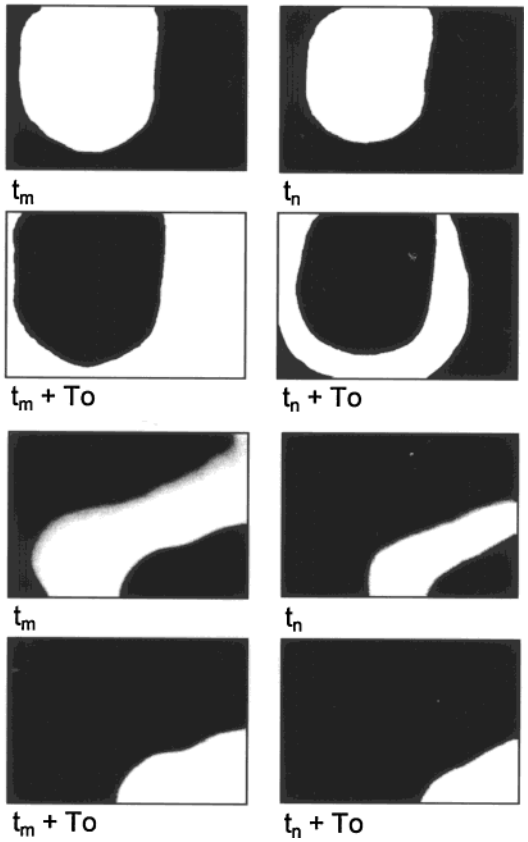


**Figure 3.** Snapshots of standing clusters (SC) and localized clusters (LC) separated in time by one period of global oscillations, $T_0$. (a) LC are obtained from SC by increasing $g$ from 55 (left snapshots) to 136 mM$^{-1}$ (right snapshots), $T_0 = 36$ s for $g = 55$ mM$^{-1}$ and $T_0 = 40.5$ s for $g = 136$ mM$^{-1}$. (b) Shrinkage of LC with an increase in $g$ from 110 (left snapshots) to 163 mM$^{-1}$ (right snapshots). Initial reagent concentrations for (a) and (b) correspond to cases a and d in Table 1, respectively.

global oscillations, are shown in Figure 5. In snapshots "999" and "1001" we show the time evolution in more detail. The domains in these patterns slowly shift and change form. First, white domains emerge in the area formerly occupied by black domains, as in the case of SC. Then, with a small delay (or phase shift), new, gray domains appear in the area adjacent to the existing white domains. The phase shift between the white and gray domains is about 3 s, while the period of global oscillations is about 20 s. Local oscillations in [Ru(III)] at two different points "1" and "2" (curves "1" and "2", respectively) are shown in the lowest part of Figure 5. The small phase shift between the white and gray domains is seen in the time intervals 830−850, 895−910, and 955−970 s, when points "1" and "2" belong to two adjacent white and gray domains. At moments $t = 863$ s and $t = 882$ s, one of the marked points belongs to black domains, and one of the corresponding curves "1" or "2" has no maximum at these moments of time. The local amplitude of oscillation in the gray domains is smaller than in the white domains, because the gray domains start to arise when the light is already turned on (light decreases the amplitude of oscillations). At $t = 921$ s and $t = 982$ s, both marked points lie in black domains. All maxima of curves "1" and "2" coincide with maxima of the global curve "3".

These three-phase clusters (3pC) differ from the 3pC found by Petrov et al.,[22] in which the phase shift between clusters is $2\pi/3$. Our 3pC resemble two-phase standing clusters in which the white domains are split into white and gray subdomains. This splitting leads to an instability of the 3pC, which can be

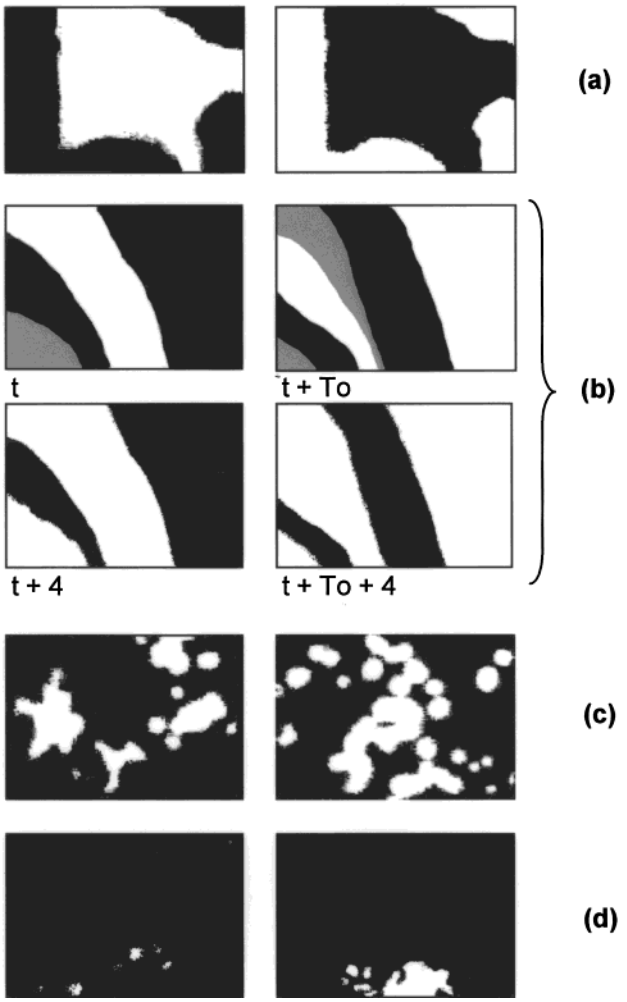


**Figure 4.** Snapshots of (a) standing clusters, (b) 3-phase clusters, (c) irregular clusters, and (d) localized irregular clusters taken at consecutive maxima (except case b) of global oscillation ($U$ - $U_{Ref}$). In (b), symbols under frames show time in seconds, $T_0 = 21$ s. Feedback coefficient $g$ ($mM^{-1}$) equals (a) 136, (b) 144, (c) 150, (d) 272. Initial concentrations correspond to case f in Table 1.

seen in the irregular local oscillations in curves "1" and "2" of the bottom panel of Figure 5.

IC and LIC are complex and interesting objects. On one hand, white domains appear and disappear periodically. The power spectrum of $I/I_{max}$ for an IC is presented in Figure 6a; a sharp peak is clearly seen, corresponding to the frequency of global oscillations, or of white domain appearance. On the other hand, where the white domains appear in space in previously dark areas is unpredictable. What is certain is that a white domain will not arise in an area that was white during the previous period of global oscillation. Figure 6b presents two consecutive snapshots of an IC and the result of their summation. No white domains overlap. Using image analysis techniques we verified that white domains of two consecutive periods of an IC never overlap. This behavior is a consequence of the antiphase oscillations of the clusters. If two snapshots are separated by several periods of global oscillation, however, their white domains may overlap, as in the lower right panel of Figure 6b.

To characterize the spatiotemporal behavior of IC, we introduce the correlation function $f_{corr}(n)$,

$$f_{corr}(n) = \left\langle \frac{p(t_m, t_m + nT_0)}{p(t_m)\, p(t_m + nT_0)} \right\rangle - 1 \qquad (2)$$

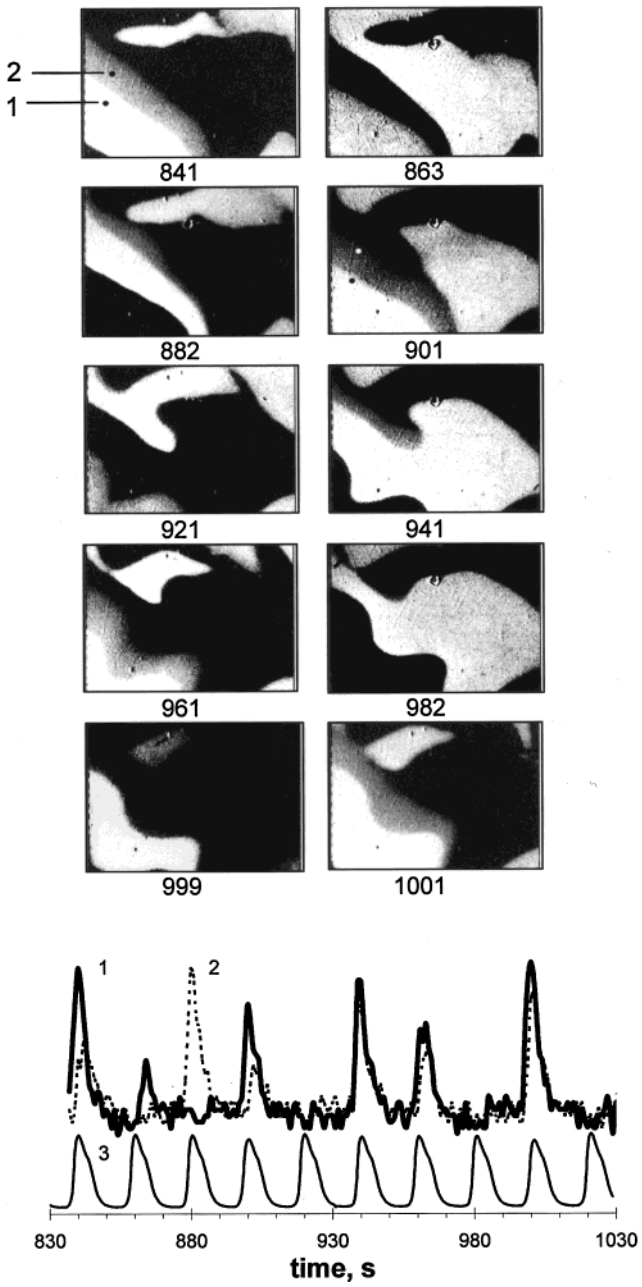


**Figure 5.** Three-phase clusters. Snapshots are taken at successive maxima of global oscillations of $[Ru(III)]_{av}$ shown in curve 3 of bottom panel. Numbers under snapshots are time in seconds. Local oscillations (arbitrary units) at points "1" and "2" indicated in snapshot "841" are shown in curves "1" and "2" in bottom panel. The same points are also indicated in snapshot "901". Initial concentrations correspond to case *f* in Table 1, $g = 144$ $mM^{-1}$, $T_0 = 20.1$ s.

where $n$ is the number of global oscillations since some initial moment of time $t_m$, corresponding to the $m$th maximum of $I$ (or Abs-450); $p(t_m)$ and $p(t_m + nT_0)$ are the fractions of the snapshot area occupied by white domains at $t_m$ and $t_m + nT_0$, respectively; and $p(t_m, t_m + nT_0)$ is the fraction of overlapping white area of snapshots taken at $t_m$ and $t_m + nT_0$. The symbol $\langle\ \rangle$ signifies an average over $t_m$. If the location of white domains in the next period of oscillation is random and has no correlation with the previous white domains, then $f_{corr}(n) = 0$. The correlation function for a typical SC is presented in Figure 6c. Correlation functions for IC and LIC are presented in Figure 6c and e. For LIC, the fractions $p()$ are calculated based on the area of the oscillatory region (region that can be occupied by white

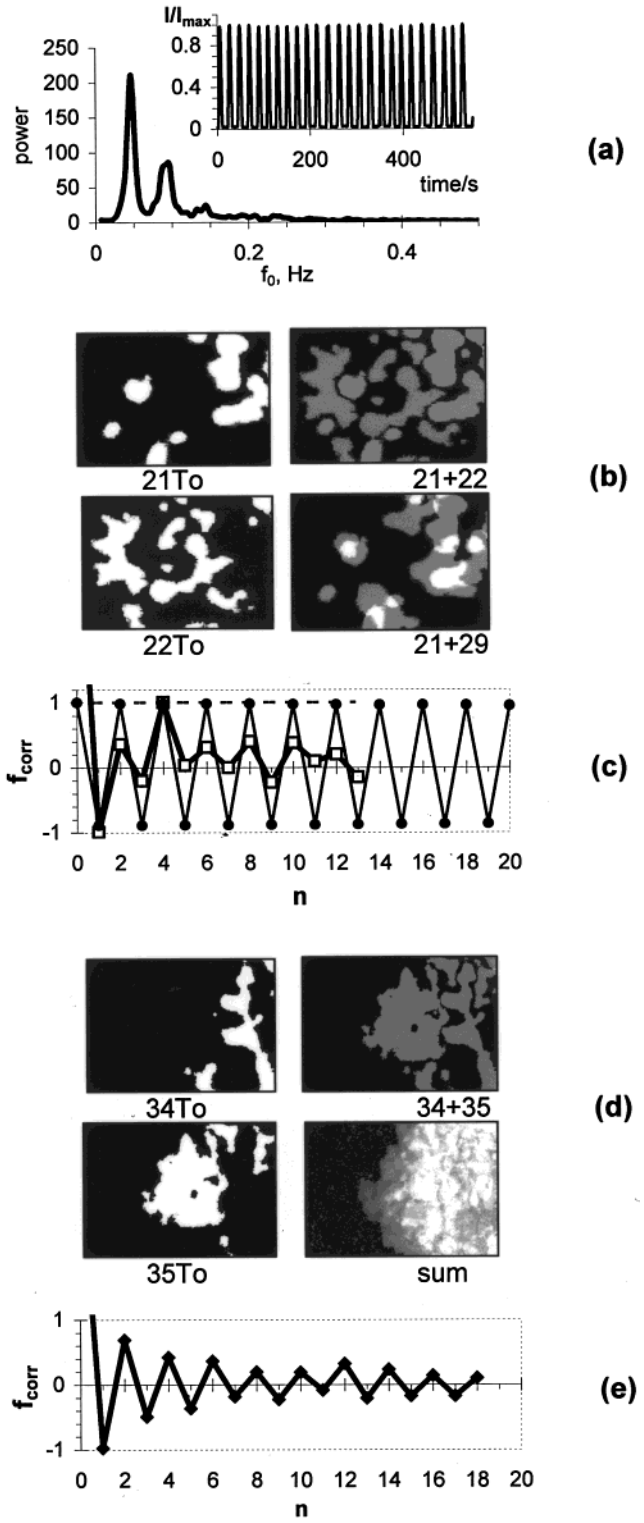


**Figure 6.** Characteristics of irregular clusters (IC). (a) Fourier spectrum of oscillations of actinic light (inset) for IC shown in b. Parts c and e show spatiotemporal correlation functions $f_{corr}$ (thick line in c) for IC (b) and localized IC (d), respectively. Thin line in c is $f_{corr}$ for standing clusters shown in Figure 7d. Initial concentrations for IC and LIC correspond to cases f and e in Table 1, respectively, $g$ ($mM^{-1}$) = (b) 150, (d) 136. Top right images in b and d are summation of consecutive snapshots in left side of corresponding parts. Right bottom image in b is summation of two snapshots separated in time by 8 periods of global oscillation. Right bottom image in d is summation of 56 snapshots of LIC, on the basis of which we calculated $f_{corr}$.

domains) rather than on the total area of the frame. This area is calculated from a summation of many snapshots of the LIC (see bottom right panel in Figure 6d). The correlation functions for IC and LIC indicate that any two consecutive snapshots have zero overlapping white area, $f_{corr}(1) = -1$. The degree of correlation decreases with $n$ and tends to 0 as $n \rightarrow \infty$. Correlation persists even for $n \geq 10$. The correlation function for IC shows a surprising maximum at $n = 4$ that merits further investigation.

Typical examples of SC obtained from nonuniform initial conditions are presented in Figure 7. Snapshots a and d were obtained by instantaneously switching on the feedback on after (a) wave and (d) spiral patterns had developed in the gel without illumination. Patterns b and e grew in a gel initially illuminated through spot and stripe masks, respectively, with constant light for 30 s. In case d, a large increase in $g$ leads to the deformation of SC but cannot induce the transition from SC to LC or to IC (see Figure 7f). The light intensity $I$ and $(U - U_{ref})$ for b are shown in the bottom panel of Figure 7. It is clear that the period of SC is $2T_0$. Successive peaks have unequal amplitudes, because the areas occupied by white and black domains are different. The SC for concentrations $h$ and $j$ in Table 1 are extremely stable. For example, after 100 or more periods of oscillation we saw no significant changes in the shape of the SC presented in Figure 7d. We did not observe similar stability for SC in cases a−d in Table 1.

At higher $g$, a new pattern is found in case $h$ (Figure 7c). This pattern has features of both SC and bulk oscillations. Part of the gel area oscillates as a unit during each period, while the remainder of the gel displays localized standing clusters with nodal lines. The local oscillations in the left and right parts of the gel area have different periods, $2T_0$ for the left side and $T_0$ for the right side. Patterns of this type may be dubbed localized oscillatory clusters (LOC). In "ordinary" LC, a portion of the gel area does not oscillate (or oscillates with very small amplitude) and shows fixed black domains at all times. In LOC, the noncluster region oscillates with large amplitude.

Ideal standing clusters are characterized by domains oscillating in antiphase and separated by fixed nodal lines or narrow zones. Under certain conditions, these nodal lines may evolve in time. Figure 8 shows a striped SC with moving nodal lines. The movement of the boundaries between black and white domains in the direction from white to black is clearly seen in the central panel of the figure. When $(U - U_{Ref})$ and $I$ are small, the velocity of boundary movement (trigger front) is high. At this stage, white domains spread as phase waves. When $I$ reaches the critical value $I_2$, the propagation of boundaries slows down and finally stops, as the white domains start to disappear. The two right images in Figure 8 reveal that white domains separated in time by one period $T_0$ do not overlap in snapshots taken before $(U - U_{Ref})$ reaches its maximum, but do overlap if snapshots are taken after this time. The overlapping area oscillates at the frequency of global oscillation, while the main area of antiphase domains oscillates at half that frequency. These oscillations resemble those in LOC, except that here the area oscillating with double frequency is quite small. This example demonstrates that the narrow zones that separate antiphase domains of clusters differ from the fixed nodal lines of standing waves. In standing waves, nodal lines are fixed and do not move at all. In the case of clusters, narrow boundary zones between antiphase clusters may oscillate with double frequency, belonging to one cluster for the first half period and to the neighboring cluster in the second half period.

Another aspect of nodal line motion involves the shape of the domains. Nodal lines with different curvatures move with

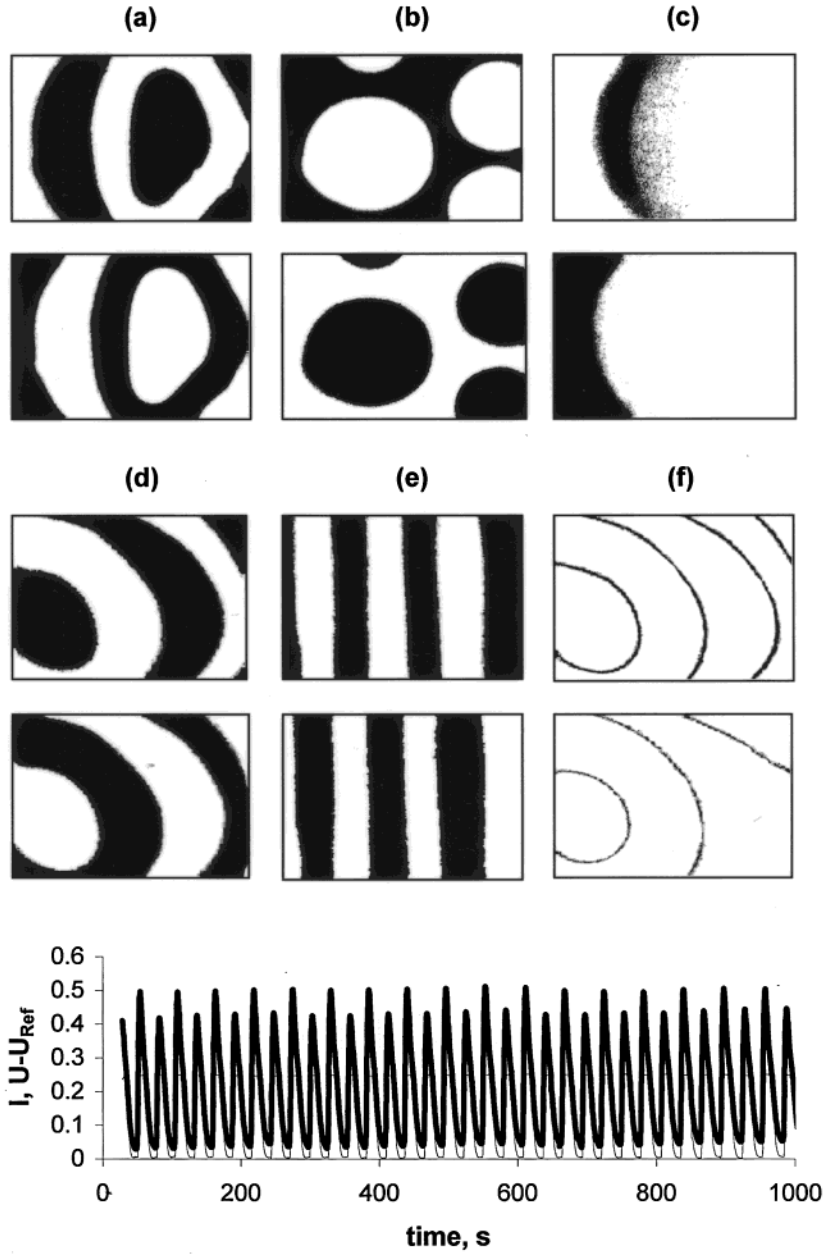


**Figure 7.** Couples of antiphase snapshots for standing clusters (a, b, d, e), localized oscillatory clusters (c), and summations of two consecutive snapshots of SC (f) separated by one period of global oscillation for $g = 27$ (top image) (corresponds to d) and $g = 163$ mM$^{-1}$ (bottom image). Initial concentrations for a−c and d−f correspond to cases h and j in Table 1, respectively. SC for cases b and e are obtained by using mask to define spatial initial conditions. SC in cases a and d are obtained from wave patterns in the gel as initial conditions. LOCs in c are obtained from a by increasing feedback coefficient $g$ from 19 to 55 mM$^{-1}$. $g$ (mM$^{-1}$) = (a) 19, (b, (d) 27, (c, e) 55. Bottom part shows ($U - U_{Ref}$) (bold line) and $I$ (thin line, relative units) for spotlike SC in b.

different speeds. We postulate that the eikonal eq 3 for the velocity of traveling curved waves (trigger waves)[42] holds for the movement of nodal lines:

$$v = v_0 - Dk \tag{3}$$

where $v_0$ is the velocity of a planar front, $k$ is the local curvature, and $D$ is the effective diffusion coefficient. The curvature $k$ is positive if an arc of a circle moves away from the center of the circle. Equation 3 implies different velocities for curved nodal lines travelling in opposite directions. For example, the velocity of an expanding white spot is smaller than the velocity of a shrinking black spot. This difference in boundary velocity leads to the disappearance of small spots and sharp angles as well as a smoothing of the boundaries between black and white domains. In general, the average curvature of nodal lines in clusters tends to decrease.

For case *k* in Table 1 (parameters close to the Hopf bifurcation line between the oscillatory and oxidized steady state regions), we failed to find clusters. A typical example of the patterns found in this case is presented in Figure 9. The white spots of this pacemaker pattern appear at the same location in each period of global oscillation. They grow, then they are suppressed by light and disappear. Thus, not every point in the oscillatory region of the parameter space gives rise to clusters. This particular point is characterized by a relatively long period ($T = 64$ s), sinusoidal-like oscillations and a large fraction of the cycle when the system is in the oxidized state. During this time [Br$^-$] rises to relatively high levels. Perhaps this concentration of bromide ions is comparable to the level reached in the

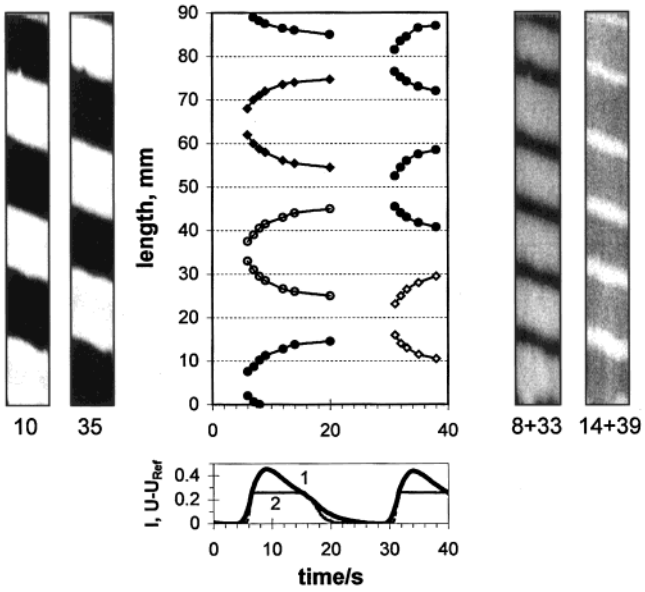


**Figure 8.** Moving boundaries between black and white domains of SC. Central panel shows dependence of boundary position on time at fixed $x$ (horizontal)-coordinate of snapshots. Initial concentrations correspond to case $h$ in Table 1, $g = 27$ mM$^{-1}$. Frame size is 90 × 70 mm$^2$ (different scales for width and height). Left two snapshots are taken at $t = 10$ s and $t = 35$ s. These moments of time correspond to maxima of $(U - U_{Ref})$ oscillations (bottom panel, curve 1; curve 2 is light intensity in arbitrary units). Right two images are summation of snapshots taken at $t = 8$ s and $t = 33$ s (before maxima); and $t = 14$ s and $t = 39$ s (after maxima). Overlapped black (white) domains give black (white) color; overlapped black and white domains give gray color.

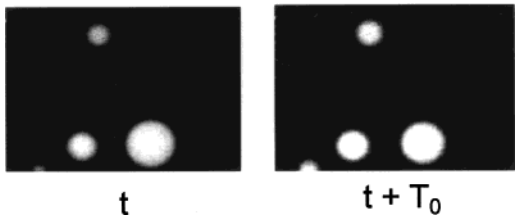


**Figure 9.** Snapshots of pacemaker-type patterns separated in time by one period of global oscillations. Initial concentrations correspond to case $k$ in Table 1. Patterns do not change by varying $g$ from 14 to 110 mM$^{-1}$.

case of constant illumination when the system "forgets" its state in the previous period of oscillation and goes to a more or less uniform reduced state.

Transitions between different types of clusters may be induced not only by changing $g$, but also by varying $Z_t$. In another set of experiments, we allowed $(U - U_{Ref})$ to become negative subject the conditions that a) if $U - U_{Ref} < 0$, $I_{act} = 0$ and (b) if $Kc(U - U_{Ref}) > \pi/2$, $I_{act} = I_{max}$ (see eq 1). In this case we obtained a square light intensity profile and were able to vary the ratio between the light and dark periods of illumination, $\tau_l/\tau_d$ (see bottom panel in Figure 10). A decrease in $U_{ref}$ leads to an increase in the duration of the light phase of illumination and consequently to an increase in bromide ion concentration in the gel. All types of cluster−cluster transitions may be caused by varying $\tau_l$ or $\tau_l/\tau_d$. It is not possible to change only one of the parameters, e.g., $\tau_l$, since the period of global oscillations, $T_0$, $(T_0 = \tau_l + \tau_d)$ increases nonlinearly with $\tau_l$. Examples of pattern transitions at constant $g$ are presented in Figures 10 and 11. The transition from SC to LC is shown in Figure 10a. In this case, $\tau_l$ and $\tau_l/\tau_d$ are increased from 2.2 s and 0.32, respectively, to 3 s and 0.43. Larger increases in $\tau_l$ and $\tau_l/\tau_d$

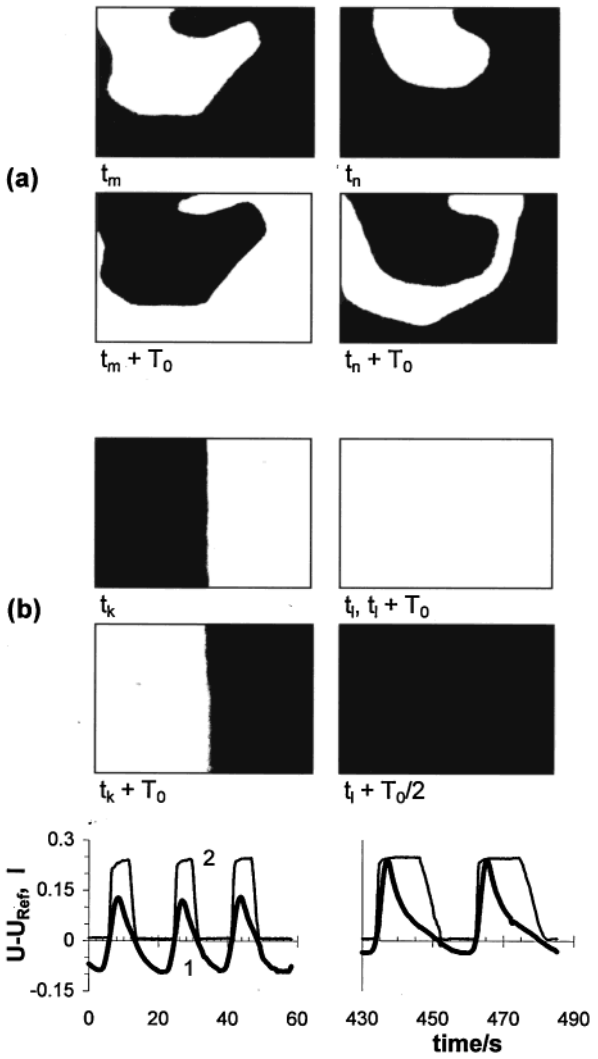


**Figure 10.** Snapshots of standing clusters (SC), localized clusters (LC), and bulk oscillations taken at consecutive maxima of $U - U_{Ref}$. (a), LC (two right snapshots) obtained from SC (two left snapshots) by decreasing $U_{Ref}$ by 20 mV at $g = 55$ mM$^{-1}$. (b) Bulk oscillations (two right snapshots) obtained from SC (two left snapshots) by decreasing $U_{Ref}$ by 90 mV at $g = 27$ mM$^{-1}$. Moments of time $t_m$, $t_n$, $t_k$, and $t_l$ correspond to maxima of $U - U_{Ref}$. Initial concentrations for a and b correspond to cases $a$ and $d$ in Table 1, respectively. In bottom part, curve 1 (bold) is $(U - U_{Ref})$ in V, and curve 2 is light intensity in relative units for case b. Left (right) graph corresponds to left (right) parts in b.

(from 5 s and 0.4, respectively, to 13 s and 0.81) completely suppress cluster formation and lead to the emergence of bulk oscillation (Figure 10b). The transition from SC to IC at constant $g$ is shown in Figure 11. In this case, $\tau_l$ and $\tau_l/\tau_d$ are increased from 4.8 s and 0.33, respectively, to 12.2 s and 0.69.

## IV. Simulations

Detailed simulations of the BZ reaction with global feedback [23,43] revealed that a two-dimensional homogeneous system exhibits the following scenario of pattern bifurcations with increasing feedback coefficient: bulk oscillations-traveling waves → standing clusters → irregular clusters → localized clusters → small-amplitude bulk oscillations. LC were found only for initial reagent concentrations close to the Hopf line. The description "bulk oscillations-traveling waves" means that bulk oscillations are a stable solution of the homogeneous reaction−diffusion model system without imperfections. Any

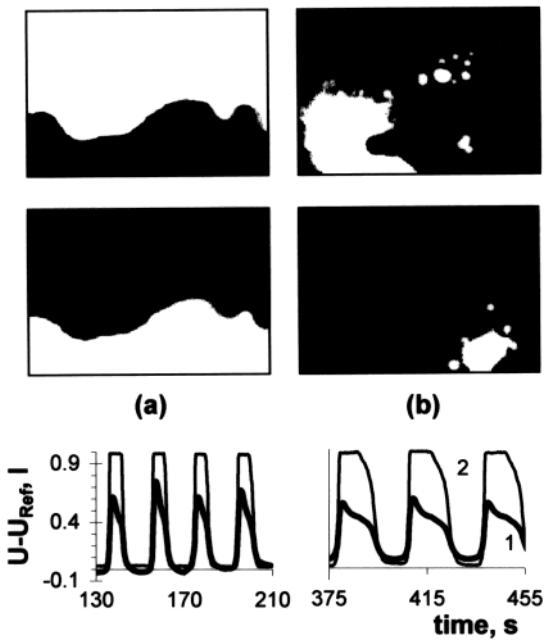


**Figure 11.** Snapshots of (a) standing clusters and (b) irregular clusters taken at two consecutive maxima of ($U$ - $U_{Ref}$) at constant $g = 136$ $mM^{-1}$. Snapshots (b) are obtained from (a) by decreasing $U_{Ref}$ by 100 mV. Initial concentrations correspond to case *f* in Table 1. Curve 1 is ($U - U_{Ref}$) and curve 2 is light intensity in relative units. Left (right) graph corresponds to left (right) parts.

small defect, however, leads to transition from bulk oscillations to traveling waves, as occurs in experiment.

The goal of this section is to establish the bifurcation scenario for simple systems consisting of several (2, 3, or 4) identical oscillators globally coupled through negative feedback without diffusion terms. In this model, SC correspond to modes in which all units oscillate and at least one is out of phase with the rest. LC may be represented as three oscillators, two of them showing high-amplitude antiphase oscillations and the third oscillating with small amplitude. This last oscillator corresponds to those parts of the gel in which there are no visible patterns. IC are similar to chaotic oscillations, which are easily obtained in a system of three coupled oscillators.[44,45]

As the simplest model of the BZ reaction we choose the Oregonator model[46] for the individual oscillators. The negative global feedback mimics that in the experiment, with the rate of additional production of the inhibitor Y in each oscillator proportional to the average of *Z*. Our model equations are

$$d[X_i]/dt = k_1[A][Y_i] - k_2[X_i][Y_i] + k_3[A][X_i] - 2k_4[X_i][X_i] \quad (O1)$$

$$d[Y_i]/dt = -k_1[A][Y_i] - k_2[X_i][Y_i] + fk_5[B][Z_i] + gZ_{av} \quad (O2)$$

$$d[Z_i]/dt = 2k_3[A][X_i] - k_5[B][Z_i] \quad (O3)$$

where $Z_{av} = \sum[Z_i]/N$, $f = 0.5$, $k_1 = 0.2$ $M^{-1}$ $s^{-1}$, $k_2 = 2 \times 10^5$ $M^{-1}$ $s^{-1}$, $k_3 = 20$ $M^{-1}$ $s^{-1}$, $k_4 = 2 \times 10^3$ $M^{-1}$ $s^{-1}$, $k_5 = 1$ $M^{-1}$ $s^{-1}$, [A] = 0.1 M, and [B] = 1 M. Initial conditions for all oscillators are approximately the same, with a very small phase shift between oscillators.

Bifurcation diagrams for $N = 3$ and $N = 2$ and examples of the most common behaviors for $N = 3$ are presented in Figure 12. Other types of system behavior for $N = 2-4$ appear in the Supporting Information. The bifurcation scenario for $N = 3$ is the same as that in the case of the spatially extended BZ system: 1-phase (bulk oscillations) → 2-phase (SC) → 3-phase (3pC) → chaos (IC) → local (LC) → small-amplitude in-phase oscillations. This is our most striking result. The bifurcation scenario for $N = 4$ is very close to that of $N = 3$.

In Table 2 we summarize the results of our simulations for $N = 2-4$. When $g$ ($s^{-1}$) ranges between 0 and 0.0094, all oscillators are in phase (1-phase). At $g = 0.0095$, a splitting ($S - 1$) occurs and period of oscillations is doubled. For $N = 3$, three slightly shifted peaks with slightly different amplitudes can be seen. For $N = 4$, the oscillators are grouped as two couples with slightly shifted peaks; the oscillators in each couple are in phase. At $g = 0.012-0.015$, the system is in a two-phase state for all $N$. For $N = 2$, the two oscillators are out of phase with a symmetrical phase shift ($\pi$). This state does not change up to $g = 0.095$. For $N = 3$, two oscillators are in phase; for $N = 4$, three oscillators are in phase. The amplitude of the in-phase oscillators is slightly smaller than that of the remaining oscillator. The phase shift between peaks is not symmetrical (for $N = 3$, approximately $0.8\pi$ and $1.2\pi$, for $N = 4$, $4\pi/3$, and $2\pi/3$). At $g = 0.0155$, the second splitting (S-2) occurs for $N = 3$ and $N = 4$. In-phase oscillators are split, and their period of oscillations is doubled again (see diagram in Figure 12). At $g = 0.018-0.074$ both systems ($N = 3$ and $N = 4$) are in a three-phase regime. For $N = 3$, the phase shift between peaks is symmetrical ($2\pi/3$). For $N = 4$, two oscillators remain in phase, and the phase shift between peaks is not symmetrical ($0.6\pi$, $0.57\pi$, and $0.83\pi$). For $N = 4$ at $g = 0.075-0.076$, the system exhibits a complex behavior we refer to as "beating". For many periods, the system oscillates approximately periodically with different amplitudes for each oscillator and with phase shifts between oscillators. Then, the individual oscillator amplitudes change, and after a short period of irregular oscillations a new periodic regime is established. The chaotic regime starts after the beating regime for $N = 4$ and after the three-phase regime for $N = 3$.

The localized oscillations are characterized by two frequencies for the two groups of oscillators, $f_1 = 2f_2$, and significantly different amplitudes ($A_1 < A_2$). For $N = 3$, the peaks of the small-amplitude, high-frequency oscillator coincide in time with the peaks of the other two single oscillators, with $A_2/A_1 = 2.4$ (see Figure 12). For $N = 4$, two oscillators oscillate in phase with small amplitude, and their peaks occur between the peaks of the other two oscillators, with $A_2/A_1 = 7$. Between the chaotic and localized regimes there is a narrow range of $g$ at which a complex periodic state of the entire system exists. For example, for $N = 3$ and $g = 0.092$, the period of each oscillator is equal to 307 s (4 times longer than the period of an isolated oscillator). For $N = 4$ at $g = 0.09-0.0922$, a very small change in $g$, about 0.0001, leads to either a 4-phase regime with period $T = 386$ s, in which each oscillator undergoes identical cycles of large and small amplitude oscillation, or to localized oscillations similar to those found for $g = 0.0925-0.0945$. When $g$ exceeds 0.095, the system transforms to the small-amplitude in-phase regime at all $N$. Since the minimum value of [Z] is greater than zero, the feedback term $gZ_{av}$ brings the system to the steady state at $g > 0.1$.

## V. Discussion

We have studied the spatially extended oscillatory BZ reaction with global negative feedback. This system may be viewed as an ensemble of locally and globally coupled microoscillators. There exist several theoretical studies of globally coupled oscillators,[47−49] globally coupled maps,[50] and globally coupled

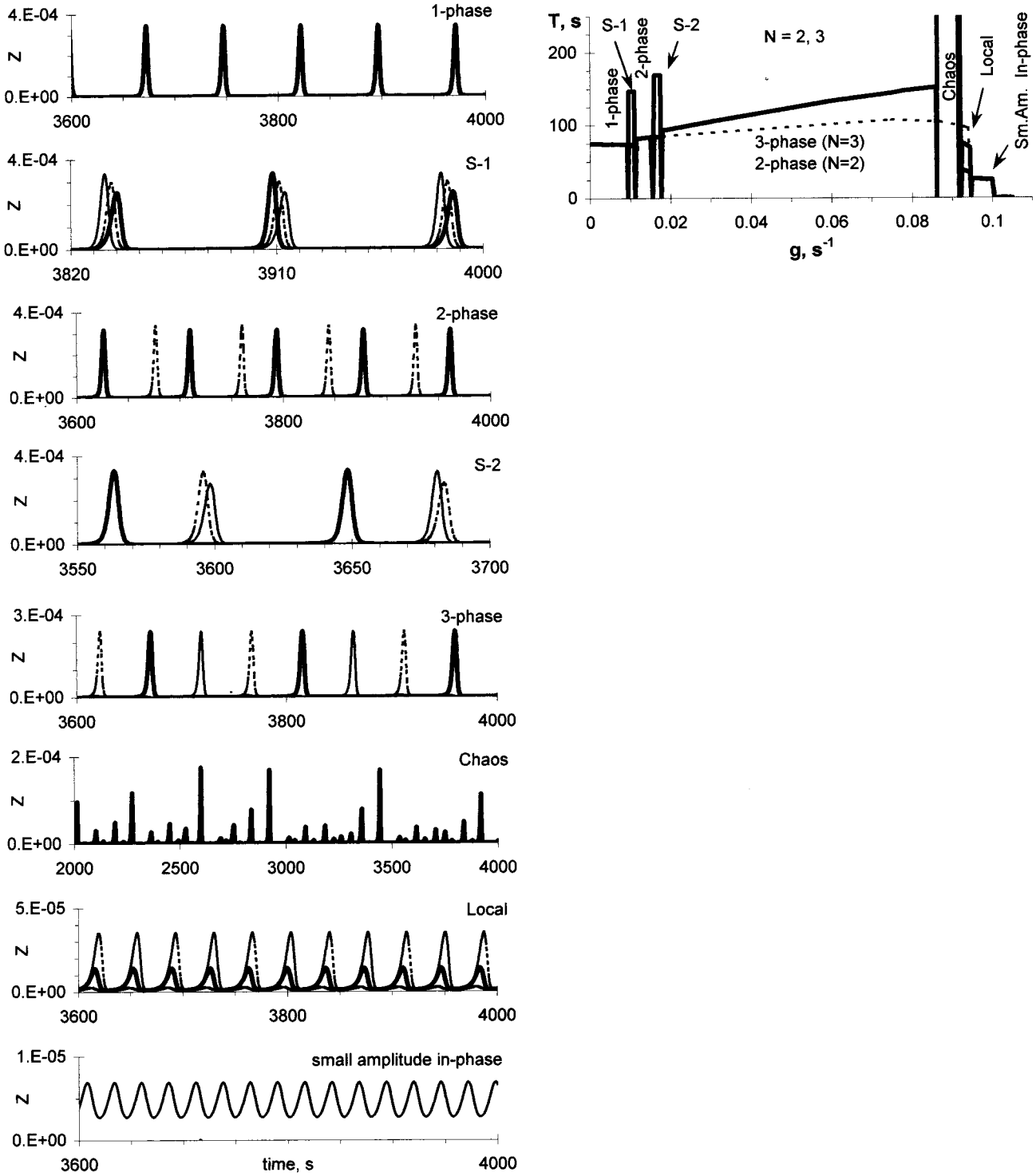


**Figure 12.** Bifurcation diagram showing dependence of period of oscillations $T$ on the feedback coefficient $g$ for $N = 3$ (thick line) and $N = 2$ (thin dotted line), and examples of primary behavior for $N = 3$. In diagram, S-1 and S-2 are splitting-1 and splitting-2 regimes. Examples of system behavior: 1-phase ($g = 0.003$ s$^{-1}$), S-1 ($g = 0.011$ s$^{-1}$), 2-phase ($g = 0.0145$ s$^{-1}$), S-2 (g = 0.0175 s$^{-1}$), three-phase ($g = 0.075$ s$^{-1}$), chaos ($g = 0.087$ s$^{-1}$), local regime ($g = 0.093$ s$^{-1}$), and small amplitude in-phase regime ($g = 0.096$ s$^{-1}$).

complex Ginzburg−Landau equations.[13,14,48] The general result of these works is that three primary types of system behavior can be achieved by varying the strength of global coupling: in-phase or uniform oscillations, clustering, and chaotic behavior of averaged variables[48] or wave-induced chaos (chemical turbulence).[14,51] Our experimental result is similar to these theoretical predictions. By changing $g$ or the target point $Z_t$ we have found three main types of behavior: waves, clusters, and bulk oscillations. We have seen the following scenario for cluster−cluster bifurcations in the spatially extended BZ reaction as the strength of global coupling increases: standing clusters → three-phase clusters → irregular clusters → localized irregular clusters → localized clusters → localized oscillatory clusters. The position of localized oscillatory clusters in this sequence is not yet precisely defined. Depending on the initial reagent concentrations (or on the position of the working point in the oscillatory parameter region), some elements of this bifurcation cascade may be absent.

We believe that this scenario is fundamental and may be found in other chemical and biological spatially extended

**TABLE 2: Bifurcation Sequence in Systems of *N* Identical Oregonators with Global Negative Feedback**

| $g$, $s^{-1}$ | $N = 2$ | $N = 3$ | $N = 4$ |
|---|---|---|---|
| 0−0.0094 | 1-phase | 1-phase | 1-phase |
| 0.0095−0.011 | splitting-1 | splitting-1 | splitting-1 |
| 0.0115−0.0145 | two-phase | two-phase | two-phase |
| 0.0155−0.0165 | two-phase | splitting-2 | splitting-2 |
| 0.017−0.0177 | two-phase | splitting-2 | three-phase |
| 0.018−0.074 | two-phase | three-phase | three-phase |
| 0.075−0.076 | two-phase | three-phase | beating |
| 0.078−0.086 | two-phase | three-phase | chaos |
| 0.0865−0.0895 | two-phase | chaos | chaos |
| 0.09−0.0915 | two-phase | chaos | four-phase and local |
| 0.0916−0.0922 | two-phase | complex periodic | four-phase and local |
| 0.0925−0.0945 | two-phase | local | local |
| 0.095−0.1 | small-amplitudein-phase | small-amplitudein-phase | small-amplitude in-phase |
| 0.101− | steady state | steady state | steady state |

systems. A similar scenario has been found in a ring array of electrodes under potentiostatic conditions at various values of the applied potential: waves → anti-phase oscillations → chaos → coherent oscillations.[7] This one-dimensional discrete system with mixed local and global coupling is quite different from our homogeneous reaction−diffusion system with global coupling, but the patterns obtained are analogous to ours: the antiphase oscillations and chaos correspond to standing clusters and irregular clusters, respectively, in our experiments.

We have demonstrated that the same transitions arise either from increasing $g$ or from decreasing $Z_t$. Both an increase in $g$ and a decrease in $Z_t$ lead to an increase in the light intensity averaged over an oscillation period and, consequently, to an increase in the production of bromide ions. We suggest that the effective bifurcation parameter for this system is the concentration of bromide ions generated in the gel when autocatalysis starts. The same $[Br^-]$ may be achieved at different values of $g$ (or $Z_t$) for different catalyst, BrMA, and $Br_2MA$ concentrations, gel thickness $h$, $I_{max}$, and even positions of the source of actinic light (illumination of the gel from the side of the glass window or from the side of the feeding mixture).

We also ask what are the roles of the local and global coupling in determining the bifurcation scenario. We conclude from our simulations that the global coupling is responsible for the general scenario of cluster−cluster bifurcations. The local coupling gives rise to clustering of the uniform system and the grouping of points into spatial domains, if we do not use a mask for defining the spatial initial conditions.

We consider in detail one of the most interesting cluster−cluster transitions, that between SC and IC (Figures 4 and 11), which helps to elucidate the role of local coupling and the part played by fluctuations in cluster−cluster transitions. We suggest the following mechanism for the SC−IC transition based on the fact that IC are found only for cases e and f in Table 1, when phase waves appear in the gel as small circular spots or nuclei. We denote $[Br^-]$ at points belonging to two anti-phase domains of SC as $[Br^-]_1$ and $[Br^-]_2$. Let $[Br^-]_1 < [Br^-]_2$ at $t = 0$, when $[HBrO_2]_{av}$ (or $[Ru(III)]_{av}$) is small (this situation is equivalent to the case when light is turned off in our experiment). Both $[Br^-]_1$ and $[Br^-]_2$ decrease and approach the critical value $[Br^-]_{cr}$. When autocatalysis starts in the first domain ($[Br^-]_1 < [Br^-]_{cr}$), the feedback generates bromide ions in both domains, resulting in a significant phase shift (or delay) in the start of autocatalysis in the second domain. The increase in $[Br^-]_1$ is larger than the increase in $[Br^-]_2$ because of additional reactions of Ru(III) with BrMA and $Br_2MA$ acids (reactions R1 − R3).[28,34,52] As a result, the ratio $[Br^-]_1/[Br^-]_2$ changes and soon exceeds unity.

$$Ru(III) + BrMA \rightarrow Ru(II) + BrMA^{\bullet} + H^+ \quad (R1)$$

$$2BrMA^{\bullet} \rightarrow Br^- + H^+ + CO_2 + (COOH)_2C{=}CBrCOOH \quad (R2)$$

$$Ru(III) + Br_2MA + H_2O \rightarrow Ru(II) + Br^- + \text{products} \quad (R3)$$

Owing to fluctuations, $[Br^-]$ varies at points within a single domain. Therefore, the autocatalysis starts at different points of the domain with a small phase shift, leading to the appearance of nuclei. Nuclei emerge in a formerly black domain randomly and not quite simultaneously. The radius of these nuclei $R$ is about $(D/\alpha)^{1/2}$, where $\alpha$ is determined from the exponential growth of [Ru(III)] according to $Z = Z_0e^{\alpha t}$. In Figure 4, the radius of the smallest white spots, about 0.02 cm, is 10 times larger than $(D/\alpha)^{1/2}$.

The velocity of planar trigger fronts depends on the light intensity.[41] Hence, the growth rate of the nuclei also depends on $I$. Light of high enough intensity can suppress this growth. The light intensity $I$ (and $g$) affects not only the growth rate of the nuclei but also the probability of appearance of new nuclei, since the appearance of the first nucleus leads to increased illumination of the entire gel and thus to an increase in $[Br^-]$, which suppresses the formation of nuclei everywhere in the gel. At small $g$, nuclei may grow and form large clusters, which constitute the white domains of SC. At large $g$, the growth and merging of nuclei is suppressed, and we see the small white domains characteristic of IC. The transition from the regime of growth and merging to the regime of suppression of nuclei may occur in a discontinuous manner.[53,54]

Fluctuations and inhomogeneities may play an additional role. We may think of a system with SC as composed of two antiphase oscillators. The transition from SC to 3pC, IC or LC involves a split into at least three different oscillators. This increase in the number of individual oscillators may depend both on the relation between positive local and negative global coupling and on fluctuations. Simulation of the BZ reaction−diffusion system with global coupling [23,43] revealed a wide range of $g$ at which SC (two-oscillators) and 3pC (three oscillator) coexist. In our experiments, we did not find bistability between SC and 3pC or between SC and IC. If the basin of attraction for three-oscillator behavior (3pC, IC, and LC) is much smaller than that for two-oscillator behavior (SC), or vice versa, at a particular $g$, then fluctuations may induce the transition to more stable system behavior.

**Acknowledgment.** This work was supported by the Chemistry Division of the National Science Foundation and the W. M. Keck Foundation.

**Supporting Information Available:** Behavior of $N$ identical Oregonators with global negative feedback. Figure 1-S: the dependence of $Z_{max}$ on $g$ and examples of characteristic kinetic curves for $N = 3$ and $N = 2$ at several values of $g$. Figure 2-S: the bifurcation diagram and characteristic kinetic curves for $N = 4$. Figure 3-S: characteristic kinetic curves for different regimes of four Oregonators. This material is available free of charge via the Internet at http://pubs.acs.org.

## Appendix 1

The photosensitivity of the $Ru(bpy)_3^{2+}$-catalyzed BZ reaction is determined by the rate of photoproduction of bromide ions.[34] The dependence of the photoresponse of a spatially extended BZ system on the gel thickness $h$ may be estimated from the following equation

$$d[Br^-]/dt = \varphi I/h - k_{chem}[Br^-] - (D_0/h^2)[Br^-] \quad (A1\text{-}1)$$

where $\varphi I/h$ is the rate of bromide photo production in the gel; $I$ is measured in units of photons/(cm$^2$ s) or mol/(cm$^2$ s); $\varphi$ is the quantum yield, i.e., the number of bromide ions generated per photon of incident light; $k_{chem}$ is an overall rate constant for bromide consumption; $D_0$ is the molecular diffusion coefficient of bromide ion in the silica gel; and $D_0/h^2$ is the rate constant for bromide escape from the gel to the CSTR. The steady-state concentration of $Br^-$, $[Br^-]_{ss}$, evaluated from (A1-1) has a bell-shaped dependence on $h$ with a maximum at $(D_0/k_{chem})^{1/2} \approx 0.3-0.4$ mm.

$$[Br^-]_{ss} = \frac{\varphi I}{h(k_{chem} + D_0/h^2)} \quad (A1\text{-}2)$$

Experimentally we have determined that the system is not photosensitive to light from the 150 W Xe Arc lamp at $h = 0.2$ mm. At $h \geq 0.5$, the photosensitivity of the system decreases significantly. These data are in good accord with our estimations based on eq A1-2.

## References and Notes


(1) Bar, M.; Hildebrand, M.; Eiswirth, M.; Falcke, M.; Engel, H.; Neufeld, M. *Chaos* **1994**, *4*, 499.
(2) Christoph, J.; Otterstedt, R. D.; Eiswirth, M.; Jaeger, N. I.; Hudson, J. L. *J. Chem. Phys.* **1999**, *110*, 8614.
(3) Cordonier, G. A.; Schuth, F.; Schmidt, L. D. *J. Chem. Phys.* **1989**, *91*, 5374.
(4) Ertl, G. *Science* **1991**, *254*, 1750.
(5) Falcke, M.; Engel, H. *J. Chem. Phys.* **1994**, *101*, 6255.
(6) Falcke, M.; Engel, H.; Neufeld, M. *Phys. Rev. E* **1995**, *52*, 763.
(7) Fei, Z.; Green, B. J.; Hudson, J. L. *J. Phys. Chem. B* **1999**, *103*, 2178.
(8) Graham, M. D.; Lane, S. L.; Luss, D. *J. Phys. Chem.* **1993**, *97*, 7564.
(9) Grauel, P.; Christoph, J.; Flatgen, G.; Krischer, K. *J. Phys. Chem. B* **1998**, *102*, 10264.
(10) Jakubith, S.; Rotermund, H. H.; Engel, W.; von Oertzen, A.; Ertl, G. *Phys. Rev. Lett.* **1990**, *65*, 3013.
(11) Lev, O.; Sheintuch, M.; Pisemen, L. M.; Yarnitzky, Ch. *Nature* **1988**, *336*, 458.
(12) Levine, H.; Zou, X. *Phys. Rev. E* **1993**, *48*, 50.
(13) Mertens, F.; Imbihl, R.; Mikhailov, A. *J. Chem. Phys.* **1993**, *99*, 8668.
(14) Mertens, F.; Imbihl, R.; Mikhailov, A. S. *J. Chem. Phys.* **1994**, *101*, 9903.
(15) Otterstedt, R. D.; Jaeger, N. I.; Plath, P. J.; Hudson, J. L. *Chem. Eng. Sci.* **1999**, *54*, 1221.
(16) Philippou, G.; Schultz, F.; Luss, D. *J. Phys. Chem.* **1991**, *95*, 3224.
(17) Rose, K. C.; Battogtokh, D.; Mikhailov, A.; Imbihl, R.; Engel, H.; Bradshaw, A. M. *Phys. Rev. Lett.* **1996**, *76*, 3582.
(18) Somani, M.; Liauw, M. A.; Luss, D. *Chem. Eng. Sci.* **1997**, *52*, 2331.
(19) Wang, W.; Kiss, I. Z.; Hudson, J. L. *Chaos* **2000**, *10*, 248.
(20) Otterstedt, R. D.; Jaeger, N. I.; Plath, P. J. *Phys. Rev. E* **1998**, *58*, 6810.
(21) von Oertzen, A.; Rotermund, H. H.; Mikhailov, A. S.; Ertl, G. *J. Phys. Chem. B* **2000**, *104*, 3155.
(22) Petrov, V.; Ouyang, Qi.; Swinney, H. L. *Nature* **1997**, *388*, 655.
(23) Vanag, V. K.; Yang, L.; Dolnik, M.; Zhabotinsky, A. M.; Epstein, I. R. *Nature* **2000**, *406*, 389.
(24) Vanag, V. K.; Alfimov, M. V. *J. Phys. Chem.* **1993**, *97*, 1878.
(25) Agladze, K. I.; Krinsky, V. I.; Panfilov, A. V.; Linde, H.; Kuhnert, L. *Physica D* **1989**, *39*, 38.
(26) Amemiya, T.; Kettunen, P.; Kádár, S.; Yamaguchi, T.; Showalter, K. *Chaos* **1998**, *8*, 872.
(27) Yamaguchi, T.; Kuhnert, L.; Nagy-Ungvarai, Zs.; Müller, S. C.; Hess, B. *J. Chem. Phys.* **1991**, *95*, 5831.
(28) Vanag, V. K.; Zhabotinsky, A. M.; Epstein, I. R. *J. Phys. Chem. A* **2000**, *104*, 8207.
(29) Försterling, H.-D.; Stuk, L.; Barr, A.; McCormic, W. D. *J. Phys. Chem.* **1993**, *97*, 2623.
(30) Sirimungkala, A.; Försterling, H.-D.; Dlask, V.; Field, R. J. *J. Phys. Chem. A* **1999**, *103*, 1038.
(31) Gao, Y.; Försterling, H.-D. *J. Phys. Chem.* **1995**, *99*, 8638.
(32) Amemiya, T.; Ohmori, T.; Nakaiwa, M.; Yamaguchi, T. *J. Phys. Chem. A* **1998**, *102*, 4537.
(33) Amemiya, T.; Ohmori, T.; Yamaguchi, T. *J. Phys. Chem. A* **2000**, *104*, 336.
(34) Kádár, S.; Amemiya, T.; Showalter, K. *J. Phys. Chem. A* **1997**, *101*, 8200.
(35) Mori, Y.; Nakamichi, Y.; Sekiguchi, T.; Okazaki, N.; Matsumura, T.; Hanazaki, I. *Chem. Phys. Lett.* **1993**, *211*, 421.
(36) Ram Reddy, M. K.; Slávik, Z.; Nagy-Ungvarai, Zs.; Müller, S. C. *J. Phys. Chem.* **1995**, *99*, 15081.
(37) Yamaguchi, T.; Shimamoto, Y.; Amemiya, T.; Yoshimoto, M.; Ohmori, T.; Nakaiwa, M.; Akiya, T.; Sato, M.; Matsumura-Inoue, T. *Chem. Phys. Lett.* **1996**, *259*, 219.
(38) Kádár, S.; Wang, J.; Showalter, K. *Nature* **1998**, *391*, 770.
(39) Kuhnert, L.; Agladze, K. I.; Krinsky, V. I. *Nature* **1989**, *337*, 244.
(40) Petrov, V.; Ouyang, Qi.; Li, G.; Swinney, H. L. *J. Phys. Chem.* **1996**, *100*, 18992.
(41) Ram Reddy, M. K.; Nagy-Ungvarai, Zs.; Müller, S. C. *J. Chem. Phys.* **1994**, *98*, 12255.
(42) Zykov, V. S. *Biophysics* **1980**, *25*, 906.
(43) Yang, L.; Dolnik, M.; Zhabotinsky, A. M.; Epstein, I. R. *Phys. Rev. E* **2000**, *62*. In press.
(44) Baesens, C.; Guckenheimer, J.; Kim, S.; MacKay, R. S. *Phys. D* **1991**, *49*, 387.
(45) Grebogi, C.; Ott, E.; Yorke, J. A. *Phys. D* **1985**, *15*, 354.
(46) Field, R. J.; Noyes, R. M. *J. Chem. Phys.* **1974**, *60*, 1877.
(47) Golomb, D.; Hansel, D.; Shraiman, B.; Sompolinsky, H. *Phys. Rev. A* **1992**, *45*, 3516.
(48) Hakim, V.; Rappel, W.-J. *Phys. Rev. A* **1992**, *46*, 7347.
(49) Zanette, D. H.; Mikhailov, A. S. *Phys. Rev. E* **1998**, *58*, 872.
(50) Balmforth, N. J.; Jacobson, A.; Provenzale, A. *Chaos* **1999**, *9*, 738 and references therein.
(51) Battogtokh, D.; Mikhailov, A. *Phys. D* **1996**, *90*, 84.
(52) Oslonovitch, J.; Försterling, H.-D.; Wittmann, M.; Noszticzius, Z. *J. Phys. Chem. A* **1998**, *102*, 922.
(53) Mikhailov, A. S.; Uporov, I. V. *Zh. Eksp. Teor. Fiz.* **1980**, *79*, 1958.
(54) Mikhailov, A. S.; Uporov, I. V. *Zh. Fiz. Khim.* **1982**, *56*, 606.